Università degli Studi di Milano

FACOLTÀ DI SCIENZE MATEMATICHE, FISICHE E NATURALI
Corso di Laurea in Fisica Triennale

DETERMINATION OF THE STRONG COUPLING FROM AN UNBIASED GLOBAL PARTON FIT

Tesi di Laurea in Fisica

Relatore:
Prof.
Stefano Forte
Correlatore:
Dott.
Juan Rojo

Presentata da:
Elisa Mariani
n.matricola:
706107
codice PACS:
12.38.-t

Anno Accademico 2008/09

Determination of the Strong Coupling from an unbiased Global Parton Fit

Elisa Mariani

October 7, 2009

Abstract

The aim of this work is determining the strong coupling $\alpha_s(M_z^2)$ and its uncertainty due to both experimental and procedural errors. Almost all the available hard-scattering data are used to perform global parton fits at next-to-leading order by using the NNPDF approach. We find $\alpha_s(M_z^2)= 0.1197 \pm 0.0016^{stat} \pm 0.0013^{syst}$.

Contents

Introduction

The analysis of scattering processes plays a fundamental role in the study of the structure of matter. Just like they had led to the discovery of the internal structure of the atom, at the end of the sixties scattering experiments made it possible to understand the substructure of nucleons. In the seventies it became clear that only a quantum field theory (called Quantum Chromodynamics) could properly describe the quantum-mechanical processes which take place inside nucleons. The validity of this theory has been verified and confirmed with great accuracy by scattering experiments at high energy, and can now be used to analyse new results. In QCD, the features of the nucleons are described in terms of those of their constituents. Therefore it is possible to extract from high energy scattering data information on the distribution functions describing these constituents and, from the beginning of the nineties up to now, there has been a steady improvement in the precision and variety of these data. Global analyses of these data allow the structure of the nucleons to be quantified with ever increasing accuracy. Analyses are now possible at next-to-next-to-leading order (NNLO) in the running coupling constant $\alpha s(Q^2)$. The strong coupling $\alpha_s(Q^2)$ is the only free parameter of QCD in the high energy limit, in which one can neglect quark masses. Its accurate determination is necessary for precise phenomenology. In this work we determine the coupling and the uncertainty on it from a fit to deep-inelastic scattering data. Uncertainties related to parton distributions are kept into account using the method recently proposed by the NNPDF collaboration.

1 Chromodynamics and Deep-Inelastic Scattering

1.1 Scattering experiments

Scattering experiments represent an important tool of nuclear and particle physics, since they can provide information about details of the interaction between different particles and about the internal structure of nuclei and their constituents. What happens in a typical scattering experiment is that the object to be studied (*target*) is bombarded with a beam of particles with defined energy. Occasionally a reaction of the form:

$$a + b \to x$$

occurs, where a and b denote the beam and target particles, while x denotes a final state which may contain the same particles as the initial state, but with different kinematics or different particles. By studying the final state x, it is possible to learn about the properties both of the target and of the interaction. At this point, let us distinguish between *elastic* and *inelastic* scattering.

Elastic scattering. All processes belonging to this category may be presented schematically by a reaction of the following kind:

$$a + b \to a' + b'.$$

The same particles are present both before and after the scattering. The primes indicates that the particles in the initial and final state have different energy and momenta.

Inelastic scattering. In inelastic reactions:

$$a + b \to x,$$

where the final state x contains particles which are not the same as those in the initial state. The set of allowed final states for a given initial state is determined by the conservation laws of the interaction which governs the process.

1.2 Deep Inelastic Scattering (DIS) and Structure Functions

In this thesis we will consider specifically *deep inelastic scattering* of leptons on nucleons, mediated by the electromagnetic interaction, and used as a probe of the strong interaction. The basic idea is to accelerate leptons to very high energy , then allow them to interact with strongly interacting particles (hadrons), and investigate what happens. This idea was born after

the electron had proved able to "see" protons inside the nucleus; then the following question arose spontaneously: "may the electron be able also to reveal what is inside a proton itself?". The question was answered in the affirmative by elastic scattering experiments, which were able to show that the proton is not point-like. By increasing further the energy, one reaches the *deep inelastic regime*: "deep" because, at high energies, the wavelenghts associated with the photon exchanged between the lepton and the struck hadron are much smaller than the size of the target; hence leptons can probe distances that are small compared to with the scale of the target, that is "deep" within the particle. However, the high energies tend to disrupt the target, so that it produces several new particles. This means the scattering is inelastic since the target has been changed in the process. To describe these states an invariant mass calculated in terms of the four-momenta of the exchanged photon (q) and of the incoming target (P) is used:

$$W^2 = P'^2 = (P+q)^2 = M^2 + 2Pq + q^2 = M^2 + 2M\nu - Q^2, \qquad (1)$$

where $-q^2 = Q^2$, and where we introduce the Lorentz-invariant quantity ν, defined as:

$$\nu = \frac{Pq}{M}. \qquad (2)$$

If the target proton is at rest in the laboratory system, then $P = (M, \mathbf{0})$ and $q = ((E - E'), \mathbf{q})$. Therefore we obtain:

$$\nu = \frac{M(E - E')}{M} = E - E', \qquad (3)$$

so that ν represents the energy transferred by the virtual photon (the mediator of the electromagnetic interaction) from the electron to the proton in the laboratory frame.

1.2.1 Scaling in DIS

When $Q^2 >> M^2$, many strongly interacting particles are produced. The dynamics of such production processes may be described in a similar way to that used for elastic scattering. In this latter case, the main tool was represented by *form factors*. DIS processes are instead expressed in terms of *structure functions*, which are the analogous of form factors for the inelastic case. The biggest difference in the kinematics of elastic and inelastic scattering is that , at a given beam energy E, the former can be interely represented by only one free parameter, since kinematics requires all the other parameters to depend on the free one; the description of the latter, instead involves two free parameters, since the excitation energy of the target adds a further degree of freedom. All these considerations are translated into the following mathematical expression, characterising the two scattering classes:

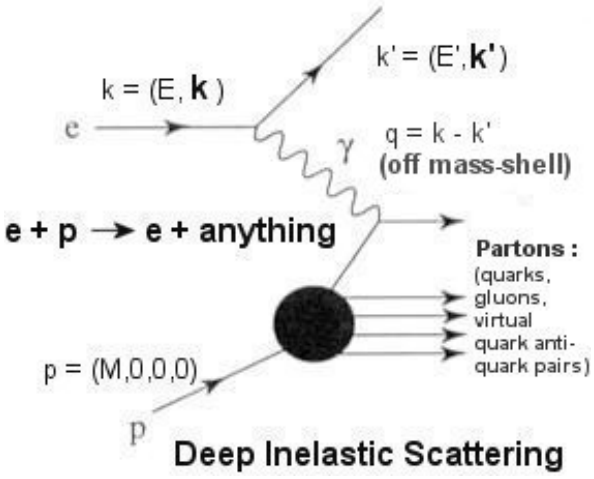

Figure 1: A graphic representation of particles production from electron-proton deep-inelastic scattering

- in the elastic case the relation $W = M$ holds, so that eq.1 yields $2M\nu = Q^2$;
- in the inelastic case, since the target aquires some excitation energy, it will necessarily follow that $W > M$, and consequently from eq.1 $2M\nu > Q^2$.

Starting with the first deep inelastic scattering experiments, which consisted of monitoring spectra of an electron scattering off hydrogen at a fixed scattering angle, carried out in the late sixties, a surprising result was found: in DIS, the structure functions F_1 and F_2 are to a good approximation independent of the scale Q^2. For scattering on a system characterized by a typical lenghtscale r, they should depend on the dimensionless combination r^2Q^2. Their scale independence (*scaling property*) thus suggests that scattering occurs on point-like constituents. To better discuss this result, a new Lorentz-invariant variable is introduced, the *Bjorken scaling variable.*

$$x := \frac{Q^2}{2Pq} = \frac{Q^2}{2M\nu}. \tag{4}$$

It is a dimensionless quantity and it represents a measure of the inelasticity of the process, since :

- in case of elastic scattering $W = M$, and consequently $x = 1$;
- whereas for inelastic scattering $W > M$, so x is constrained by the inequality $0 < x < 1$.

Dimensionless structure functions $F_1(x)$ and $F_2(x)$ have to be determined from DIS experiments, by measuring the cross-section:

$$(\frac{d^2\sigma}{dq^2 d\nu}) = \frac{4\pi\alpha^2}{q^4}\frac{E_f}{E_i M}[\frac{M}{\nu}F_2(Q^2,x)\cos^2\frac{\theta}{2} + F_1(Q^2,x)\sin^2\frac{\theta}{2}]. \qquad (5)$$

The independence of the structure functions of Q^2 suggests that electrons are scattered off a free point charge. Since nucleons are composite objects, this suggests that: *nucleons have a sub-structure made up of effectively point-like constituents.*

1.2.2 Structure functions interpretation within Parton Model

Parton model is the name given to a specific model, proposed by Feynman and Bjorken, which , on the basis of the ideas presented in the previous section, explains the scaling property of the structure functions in terms of scattering off point-like free constituents, called *partons*. Partons bearing an electrical charge are called *quarks*, whereas electrically neutral partons are called *gluons*. The model is based on one essential assumption: the scattering occurs on constituents which have momenta collinear to that of the nucleon. As a matter of fact, if one looks at the proton in a fast moving system, then transverse momenta and the rest mass of the proton constituents can be neglected, so that the proton momentum can be expressed as the sum of momenta parallel to it, i.e. those of its partons. On top of that, we introduce the *impulse approximation*: having decomposed the nucleon into an ensemble of freely moving partons, the interaction with it is assumed to be the incoherent sum of interactions with the individual partons; if we finally assume that the typical time-scale of the photon-parton interaction is so short that the interactions between the partons can be neglected, the photon-parton scattering is elastic. In this case, the Bjorken scaling variable $x = Q^2/2M\nu$ coincides with the proton four-momentum P fraction which is carried by struck parton, i.e. that parton which interacts with the exchanged photon.

We can easily compute Structure Functions within the Parton Model by introducing the distribution functions of the quark momenta $q_f(x)$, where $q_f(x)dx$ is the expectation value of the number of quarks of type f in the nucleon, whose momentum fraction lies within the interval $[x, x+dx]$. A straightforward computation then leads to:

$$F_2(x) = x\sum_f z_f^2(q_f(x) + \bar{q}_f(x)), \qquad (6)$$

where the sum is over all types of quarks and antiquarks, and z_f is the electric charge of the f-th quark. For spin 1/2 particles the following *Callan-Gross*

relation is implied:

$$2xF_1(x) = F_2(x) \tag{7}$$

If this ratio is plotted as a function of x at different values of Q^2, it can be easily seen that the ratio is, within experimental error, consistent with unity; therefore the first piece of information we get about point-like constituents of nucleons is they have spin 1/2.

1.3 QCD, asymptotic freedom and scaling violations

Quantum chromodynamics (QCD) is the quantum field of the strong interaction. It was proposed in the seventies as a description of the behaviour of the quarks inside the proton and it can be considered as an application of the ideas of gauge field theory developed in the 1960s. It is modelled upon *quantum electrodynamics* (QED), in that:

- the basic idea is to use a new charge called *colour* as the source of the interquarks forces (*chromodinamic* or *strong* forces), just as electric charge is the source of electromagnetic forces between charged particles;
- both the considered fundamental interactions take place via the exchange of a massless vector boson field, i.e. a particle with negative parity and spin 1.

In the case of QCD, these vector bosons are called *gluons*. They carry simultaneously colour and anti-colour (for example red and anti-green): in this respect QCD greatly differs from QED, where photons have no electrical charge and, consequently can't couple with each other. Gluons can couple with all colour charged particles, that is quarks, but also the gluons themselves.
From an historical point of view, *colour* was originally introduced as a new quantum number which would distinguish otherwise identical quarks and so satisfy the demands of the Pauli exclusion principle, since, soon after the proposal of the quark model, it had been realised that the suggested quark content of some particles clashed with the Pauli principle.

1.3.1 Hadrons as colour-neutral objects

Having introduced the colour charge one question arises immediately: if quarks are provided with this new charge and if they form hadrons, hadrons might be expecteded to exist in a multitude of versions differing only for total net colour, which would depend on their constituent quarks colours. But, actually, this is not the case, since only one type of each hadron is observed. This means that only particles with no net colour can exist as free

particles, consequently explaining why quarks have never been observed by themselves, as free isolated particles. Therefore, the introduction of *colour* provides a formal method of categorising which combinations of quarks and antiquarks are allowed to exist.

1.3.2 Strong coupling α_s, confinement and asymptotic freedom

In DIS experiments a remarkable effect is noticed: when the quarks are close together, the chromodynamics forces between them are weak; as the distance between them increases, so too do the forces. The term coined to denote this behaviour is *asymptotic freedom*, to indicate the fact that when the interquark distances probed become asymptotically small (that is, when the momentum of the deep inelastic probe becomes asymptotically high), then the chromodynamic forces disappear and the quarks become, effectively, free particles. On the other hand, no free quark has ever been oberved, so over long distances, the force between quarks becomes increasingly strong; this latter behaviour is called *confinement*. The existence of these two different behaviour leeds to the following considerations. The coupling constant depends on Q^2, like all couplings in quantum field theory. But, while in the electromagnetic interaction this dependence is weak at the nucleon scale, in the strong interaction it is very strong. A first-order QCD calculation yields:

$$\alpha_s = \frac{12\pi}{(33 - 2n_f)(\ln(Q^2/\Lambda^2)}, \tag{8}$$

where n_f denotes the number the number of quark types involved in pair production and depends on Q^2, because a heavy quark-antiquark pair can only be resolved at very high value of Q^2, so that $n_f \approx$3-6. Λ is the only free parameter of QCD, to be determined from comparison between theoretical predictions and experimental data. Currently it is estimated to be $\Lambda \approx 250$ MeV/c^2. Then, for very small distances among quarks, i.e. for very large values of Q^2, α_s decreases, so that interquark coupling gets weaker and weaker: in the limit $Q^2 \to \infty$, $\alpha_s \to 0$. On the contrary, when distances increase, the coupling constant increase as well and with it also interquark coupling, so that quarks can't escape. Finally, eq.8 also explains why it is so difficult to carry out reliable theoretical calculations in QCD. As a matter of fact, the application of perturbative expansion procedures is valid only if $\alpha_s << 1$. In QCD, the strenght of the chromodynamic forces, may require the quark-gluon and gluon-gluon couplings to be large (greater than one), meaning that the complicated high order processes become increasingly important. In this case, it is impossible to use the same mathematical techniques of perturbation theory to calculate quantities of physical interest. The method of perturbation theory, can then be used only in the asymptotically free regime of QCD, where the forces are weak.

1.3.3 Scaling Violations of the Structure Functions

It was previously said that structure functions are almost independent on Q^2. However this is only partly true, since high precision measurements show that to a small e from fig.2 that

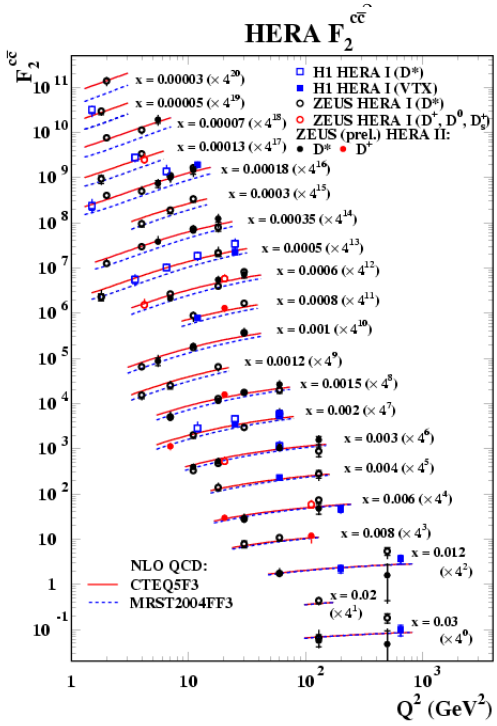

Figure 2: Structure function as a function of Q^2 at different values of x on a logarithmic scale

the structure function increases with Q^2 at small values of x, and decreases with increasing Q^2 at large values of x. This behaviour, called *Bjorken scaling violation*, means that as the momentum of the probe increases, it becomes more likely to hit a quark carrying a small fraction of the total proton momentum and less likely to hit a quark carrying a large fraction.

Now, if there are no interquark forces, then each quark in the proton will carry a well defined and constant fraction of the momentum of the proton, namely one third of this momentum, since in this simplified and static picture, the proton can be seen as made up of three quarks. However, to confine quarks inside the proton, there must be some interquark forces, even if they do weaken in effect as the distance resolved by the probe decreases to less than the proton diameter. We have already said that in QCD, forces are mediated by the exchange of gluons between the quarks. This continual exchange transfers momentum between the quarks, so that, the momentum distribution among the constituents of the nucleon is continually changing. As the momentum of the probe increases and the distance it resolves de-

creases, it begins to see the detailed quantum-mechanical sub-processes of QCD in the environment of the struck quark: if the virtual photon exchanged in a deep-inelastic scattering transfers little energy, i.e. $Q^2 = Q_0^2$ is small, then its spatial resolution will be low, so that quarks and emitted gluons cannot be distinguished and a certain quark momentum distribution $q(x, Q_0^2)$ is measured. At larger Q^2 and higher resolution emission splitting processes are visible to the photon,thus the number of partons seen to share the global momentum increases. Therefore the quark distribution $q(x, Q^2)$ measured in this case at small momentum fraction x is larger than $q(x, Q_0^2)$; obviously the effect is reversed for large x. This is the origin of the increase of the structure function with Q^2 at small x and its decrease at large x. Whereas the change in the structure functions with Q^2 can be calculated, it has so far proven impossible to predict their x-dependence in theory; it can be known only from the experiments.

2 About NNPDF

2.1 A little history of parton distribution determination

The determination of parton distribution has undergone a constant process of evolution. Initially, parton distribution were determined through a mix of model assumptions and experimental data, with the aim of comparing observed scaling violations with those predicted by perturbative QCD, thus testing the partonic interpretation of hard processes.
As the accuracy of the data increased, first parton sets , based on consistent global fits were determined at leading order , since it was accurate enough for these sets to be used in the following decade.
Then, QCD gradually entered the field of precision phyics, thanks to a second generation of high-precision deep-inelastic scattering and hadron collider experiments, and this led to the following requirements:
- determination of parton distribution at next-to-leading order (to control perturbative uncertainties);
- determination of parton distribution based on wide global sets of data coming from different experiments . Parton sets produced by different collaborations differe from each other in many technical details, but they all have a common root: a parton parametrization is originally assumed and its parameters are tuned so that the computed observables fit the experimental data.
Uncertainties are determined using standard error propagation from the covariance matrix of parameters. The choice of a functional form can be a source of theoretical bias.

In order to overcome this problem and other issues related to error propagation and data combination, a new approach to PDF determination was proposed by the NNPDF collaboration.

2.2 A brief exposition of NNPDF approach

NNPDF, which stands for "Neural Network Parton Distribution Function" is based upon two essential ingredients: Monte Carlo method, and neural network used as unbiased interpolants.
h The procedure consist of:

1. Generation of Monte Carlo ensemble of N_{rep} replicas of the original ensemble of N_{dat} data points:
   this ensemble is created following the probability distribution of the experimental data and it is large enough that the statistical properties of these data are repoduced. This means, first of all, that each replica contains as many data points as are contained in the original data set. Secondly, that the number of generated replica is such that, by

performing on the Monte Carlo ensemble statistical operations, all the original experimental information can be extracted from it: the N_{rep} ensemble of N_{dat} points are distributed around the original points in such a way that their mean value be the experimental central value and that error and covariance be equal to the correspondent experimental quantities. Because the distribution (which can be any one) of the experimental data coincides with the probability distribution of the value of the measured physical observables, the Monte Carlo set of replicas can be viewed as a sampling of the probability measure on the space of these observables. Therefore, considered one of these observables, which we indicate with the generic symbol F, the Monte Carlo generation, will produce:

$$F_i^{(art)(k)}; \quad k = 1, ..., N_{rep}, \quad i = 1, ..., N_{dat}, \tag{9}$$

values,where $F_i^{(art)(k)}$ indicates one individual measurement of F. In this case the Monte Carlo set gives a sampling of the probability distribution of the value of the structure function at the points where it has been measured, since, as it was said before, the distribution of the experimental data coincides with this probability measure. The experimental data in general consist of the determination of several physical observable in distinct experiments, each of which provides the measurement of the relevant quantity at a discrete set of values of the kinematic variables. In general there will be a non trivial set of correlations between determination of different quantities, that is between different observables at different points. Furthermore experimental data are possibly affected by errors which don't necessarily follow a gaussian distributions. Together with the existence of a non-trivial error propagation, all these facts represents the reasons why a Monte Carlo method is used, given that it is proved that to face properly this difficulties in the data treatment, it is extremely helpful to use a representation where central values are obtained from a Monte Carlo sample as averages and uncertainties as standard deviations, etc...)

2. Construction of parton distribution functions: from each data replica a set of PDF is generated by using neural networks. Given that the thoery doesn't provide a well-established functional form for PDFs, any attempt to produce a PDFs set based upon fitting a precise functional form is doomed to remain influenced by a strong theoretical prejudice which resides in this very primal choice of the functional form. The use of neural networks , which represent a form of artifical intelligence, aims at minimizing this effect. Neural networks ability to "learn" is exploited as follows: it is possible, in fact to construct a neural network with a functional form containing a huge number of parameters, and then to "train" this computational system to obtain

a final function whose form is determined by those few parameters which usually appear in a parton distribution function. This initial redundant parametrization is the only way to protect from the interference of the theoretical bias, and only neural networks are up to this specific task.

Each PDF is then parameterized at a given scale ("initial scale") by an individual neural network. More precisely N_{rep} ensemble of neural networks are constructed, where each one of them contains N_{pdf} neural networks, one for each PDF we want to determine.
The number N_{pdf} depends on the particular set of data used (at the most it can be 13, 6 for the quarks, 6 for the antiquarks and 1 for the gluon). The best fit set of PDFs is then determined for each data replica using the standard method of any parton fit, namely:

- the set of N_{pdf} functions obtained, which represents a possible candidate for this set at the initial scale, is evolved by using standard QCD evolution equations, at the scale at which data are available;
- physical observables are computed by convoluting the evolved parton distributions with hard partonic cross sections;
- the best fit is finally determined by comparing the theoretical computation of the observables for a given PDF set candidate with their replica experimental values.

The use of neural networks however requires a suitable choice of minimization algorithm, in order to deal with the large number of parameters and the nonlinear dependence on them. Of course the best fit PDFs will be different for each replica, so the ensemble of these N_{rep} best fit PDFs is the result of the fitting procedure. The N_{rep} replicas of each parton distribution provide the corresponding probability density: for example, the mean value of the parton distribution at the starting scale for a given value of x is found by averaging over the replicas, and the uncertainty over this value is the variance of the values given by the replicas.

Because neural networks are a very general functional form, their best fit to a set of data can have a very low reduced χ^2, meaning that the fit can be made to go through central data points, or almost so. This can not happen in standard data fits because of the less general functional form and it is not desirable, because one expects on statistical grounds $\chi^2 \approx 1$: if a much lower value is obtained, the fit is reproducing statistical fluctuations (*overlearning*). Therefore, even though the best fit is determined by minimizing the χ^2, it does not correspond to the absolute minimum of the χ^2. Rather, it is obtained by the *cross-validation method*. The procedure is the following:

given a replica, its data are divided randomly into two sets, one called *training set* and the other called *validation set*. At each step, during the fitting loop, two χ^2 are calculated, one for the training set data , and one for the validation set data. The χ^2 of the training set data is then minimized. The fit is stopped when the second χ^2 stops decreasing.

2.3 The importance of PDFs at LHC

The physics of parton distributions, especially within the context of DIS, has been an active subject of detailed theoretical and experimental investigations since the origins of perturbative QCD. A good knowledge of PDFs has always been vital to make predictions for both the Standard Model and beyond the Standard Model processes at hadronic colliders but now more than ever, with advent of the Large Hadron Collider (LHC) at CERN, PDFs must be known as precisely as possible, in order to maximize the discovery potential for new physics at the LHC. Conversely, of course, LHC data will lead to an improvement in the knowledge of PDFs. Since, at the LHC, proton-proton collisions will be studied, it will necessary to separate information on the proton from that on other new potential particles. This separation is possible thanks to the so-called *QCD factorization*, which at the first perturbative order, corresponds to the Parton Model. Cross-section factorization is a fundamental feature of QCD, valid at any perturbative order, and it states that the cross-section for a hadronic process can always be written as:

$$\sigma(P_1, P_2) = \sum_{i,j} \int dx_1 dx 2 f_i(x_1, \mu^2) f_j(x_2, \mu^2) \hat{\sigma}_{ij}(p_1, p_2, \alpha_s(\mu^2), \frac{Q^2}{\mu^2}), \quad (10)$$

where P_1 and P_2 are the hadron momenta, $p_i = x_i P_i$ are the momenta of the partons partecipating to the scattering, and $f_{i,j}(x, \mu^2)$ are their parton distributions. They are defined at a scale μ, called *factorization scale*, which is typically equal to the scale Q characteristic of the process. The parameter μ determines the scale at which long range physics and short range physics are separated: if a parton is emitted with a moment lower than μ, it is considered part of the hadronic structure and then absorbed in the parton distribution, whereas, a parton emitted with a moment larger or of order of than μ will be seen as part of the short-distance cross-section $\hat{\sigma}$. As long as the strong coupling α_s is small, the short-distance cross-section $\hat{\sigma}$ for the scattering of two partons i and j can be determined using perturbative calculations and, on top of that, it does not depend on the features of the hadronic wave function, which is encoded i he parton distributions. Therefore it is clear that, in order to obtain $\sigma(P_1, P_2)$ at high precision, it is necessary not only to determine $\hat{\sigma}_{i,j}$ at high perturbative order, but also to know parton distribution and their uncertainties with great accuracy.

3 Determination of the strong interaction coupling constant α_s

3.1 Motivation

The coupling constant of strong interactions (QCD) α_s is one of the fundamental parameters of the standard model (SM) of particle physics, and thus its accurate measurement is very important for precision of the SM and tests of physics beyond the SM, for instance via unification of the couplings. The value of α_s can be determined from different physical processes, as fig. 3 shows. One possible process to determine α_s is Deep-Inelastic Scattering,

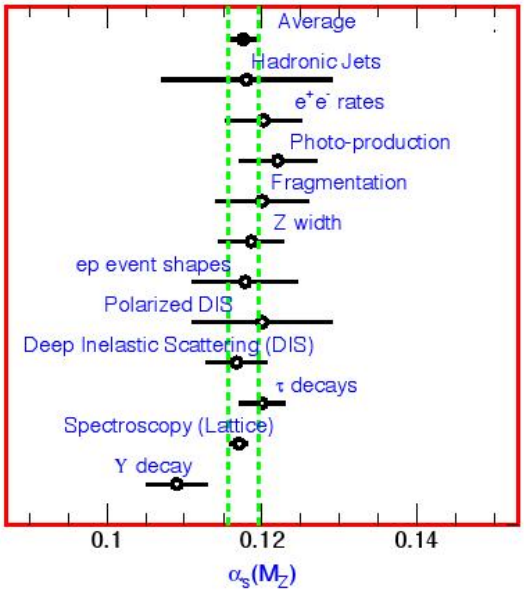

Figure 3: Summary of the value of $\alpha_s(M_z)$ from various processes. The error shown is the total error, including theoretical uncertinties.The average which comes from these measurements is also shown.(From ref.[4])

but this requires to determine simultaneously both the value of α_s and the PDFs. Therefore, an accurate determination of PDF uncertainties is necessary in order to obtain a reliable determination of α_s from DIS. The NNPDF methodology is thus suitable for this task. A summary of current determinations of α_s is shown in fig.3. As discussed in the previous section, α_s depends on the scale, and each determination will correspond to a different scale or range of scales. However, because the dependence of α_s is universal and known, all these determinations can be evolved to a common scale. By convention, the value of α_s at the scale $Q^2 = M_z^2$ is usually quoted.

3.2 Description of procedure and results

In order to determine α_s from the NNPDF global analysis, we repeat the NNPDF fit for different values of α_s. The complete procedure consists of:

1. performing the NNPDF global parton analysis for different values of α_s;
2. calculating the χ^2 for each of these partonic fits;
3. making a plot "χ^2 vs α_s" with the values obtained in the previous step;
4. checking if this ensemble of plotted points can be fitted with a curve which presents a minimum, so that in the vicinity of the minimum the χ^2 is parabolic;
5. once the condition in the previous step is verified, carrying out the parabolic fit and obtaining the minimum. This minimum will represent the value for α_s.

.

3.2.1 Check of the sensitivity to α_s of NNPDF fit

At first we check whether or not there is some sensitivity at all to α_s. To this purpose we start performing the fits by taking into consideration only three different values of the constant.
The current global average is (from ref.[4])

$$\alpha_s(M_z^2) = 0.119 \pm 0.02, \tag{11}$$

then, the first three values chosen for α_s are:

$$\alpha_s = 0.110, 0.119, 0.130, \tag{12}$$

so that the whole range of variability of α_s, within its error, is reached. The fit is performed to essentially all existing DIS data of (anti)electron, (anti)muons and neutrinos beams off proton and neutron targets. In this initial phase, we choose N_{rep}=100, whereas during the whole analysis a single Monte Carlo sampling of data will be used, to reduce fluctuations. Parton fits are based on the NNPDF1.2 parton set, which uses the NNPDF methodology and code [[5], and the data shown in fig.4. The subsequent part of the work, which involves the treatment of the global χ^2s previously obtained, is based on a large extent on the use of Root (based on C++ interpreter CINT), and, partly, on the use of C++ programs written for the purpose.
Let us display the results obtained at this initial level.

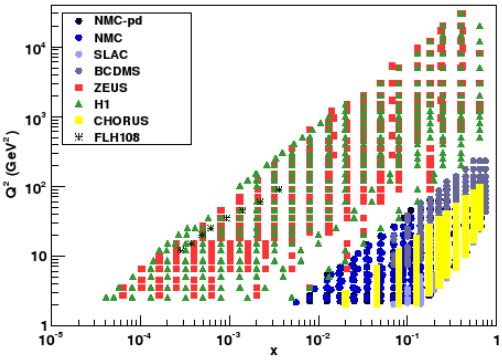

Figure 4: Experimental data representation in the (x, Q^2)

	α_s=**0.110**	α_s=**0.119**	α_s=**0.130**	*Best-fit* α_s *value*
TOT(all exp)	4640.59	4401.51	4436.57	0.123
NMC-pd	237.82	208.38	182.00	0.152
NMC	452.80	416.80	396.71	0.133
SLAC	149.25	118.47	157.53	0.119
BCDMS	908.33	901.43	954.81	0.116
ZEUS	566.71	541.13	562.95	0.120
H1	687.43	648.80	649.55	0.124
CHORUS	1378.87	1292.04	1207.90	0.163
FLH108	14.50	13.21	12.11	0.148
NTVDMN	48.76	56.37	60.58	0.133
XF3GZ	12.47	12.14	13.60	0.117
ZEUS-H2	183.64	192.73	238.82	0.111

Table 1: χ^2 of parton fits as a function of α_s value (first row on the top) and of the considered experimental set (first colum on the left).

Fig.5 clearly shows a sensitivity of the figure of merit of the fit to α_s value. The result of a parabolic fit to the total χ^2, as well as to the χ^2 of each experiment determined at these points, are collected in tab.1. The 68% CL is obtained from $\Delta\chi^2 = 1$ and it gives:

$$\alpha_s(M_z^2) = 0.123 \pm 0.0008. \tag{13}$$

Considered the data contained in tab.1, this uncertainty results unrealistically small, because:

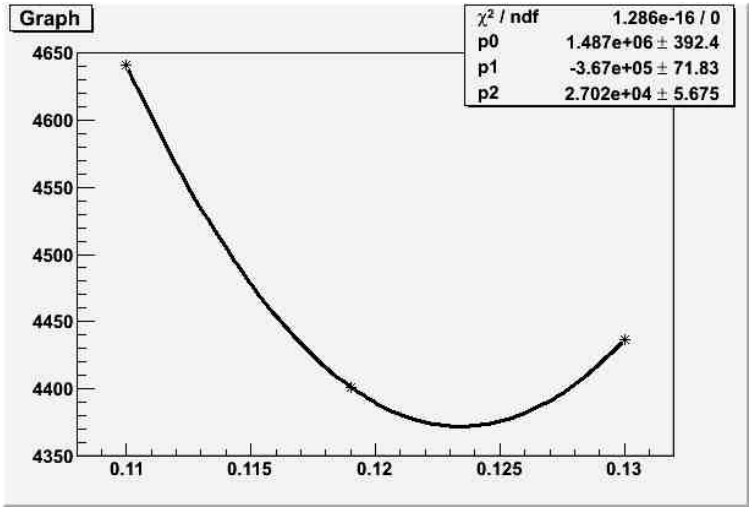

Figure 5: The parabolic fit to the total χ^2 values of tab.1.

- single experiments χ^2 are very different between each other;
- there is great variability in the *best-fit* α_s *value* of single experiments.

3.2.2 Determination of $\alpha_s(M_z^2)$ and its error

We repeat the procedure but this time with a greater number of possible values for α_s, in order to cover satisfactorily the range of variabilityof the constant. Remembering that this range was established based on the error attributed to the reference value, i.e. 0.119 ± 0.02, the following values are chosen:

$$\alpha_s = 0.110, 0.113, 0.116, 0.119, 0.121, 0.123, 0.125, 0.128, 0.130, 0.135, 0.140. \tag{14}$$

In order to get a complete survey on what happens between the extreme limits 0.110 and 0.130, the most obvious choice would have been taking 20 points equally spaced out one from another at a distance of 0.01, in order to span systematically the entire interval. Since this is computationally very intensive,we choose instead 9 points inside the cited interval (extreme limits included), plus 2 points, 0.135 and 0.140, outside it. The outer points were added because some experiments showed a minimum appreciably shifted on values greater than 0.119.

To perform the parton fits, we used N_{rep}=500. The results are collected in tab.2. A parabolic fit to the values of the total χ^2 is displayed in fig.6. Parabolic fits to the χ^2 of each experiment are shown in fig.18.

α_s	**0.110**	**0.113**	**0.116**	**0.119**	**0.121**	**0.123**
TOT(all exp)	4660.83	4595.03	4468.42	4401.74	4383.71	4384.80
NMC-pd	254.83	236.43	230.37	221.22	216.15	214.39
NMC	458.79	445.87	429.86	415.04	410.85	406.38
SLAC	152.28	134.48	122.72	117.71	118.15	124.32
BCDMS	921.49	919.20	905.39	900.63	913.88	913.51
ZEUS	569.74	573.58	549.52	543.05	539.97	540.04
H1	681.64	678.77	659.99	648.65	641.21	635.70
CHORUS	1359.41	1340.33	1306.50	1285.60	1265.64	1265.12
FLH108	14.52	14.33	13.79	13.37	12.99	12.72
NTVDMN	52.49	52.37	51.08	51.22	53.66	54.33
XF3GZ	12.44	12.25	12.25	12.30	12.36	12.55
ZEUS-H2	183.19	187.42	187.17	192.96	198.83	205.73
α_s	**0.125**	**0.128**	**0.130**	**0.135**	**0.140**	$\alpha_{s_{min}}$
TOT(all exp)	4400.62	4469.98	4562.84	5398.86	6738.84	0.120
NMC-pd	199.76	190.03	175.02	235.33	272.28	0.125
NMC	401.20	391.44	387.89	397.32	426.65	0.129
SLAC	131.99	138.85	133.88	141.08	173.16	0.122
BCDMS	921.43	974.65	1035.47	1335.34	1605.13	0.118
ZEUS	547.65	559.88	567.80	633.07	818.8	0.120
H1	640.16	644.19	667.91	793.74	1187.57	0.120
CHORUS	1262.73	1252.54	1261.37	1450.66	1735.84	0.122
FLH108	12.54	12.24	12.36	13.20	14.58	0.126
NTVDMN	55.68	59.55	61.10	88.62	117.98	0.118
XF3GZ	12.72	13.26	13.68	15.40	18.61	0.117
ZEUS-H2	214.78	233.35	246.46	295.11	368.06	0.115

Table 2: χ^2 of parton fits based on 500 replica as a function of α_s value and of the considered sperimental set. *Best-fit α_s value.*

The latter plot shows that each experiment has a minimum but that these minima can sensibly differ between each other. This great variability is due both to the fact that these experiments probe different processes in different kinematic regions and to statistical fluctuations. On top of these, there is a procedural uncertainty due to the fact that we are using a finite number of replicas. This procedural uncertainty is reflected in the quality of the parabolic fit of fig.6, which is quite poor. Based on the expected size of these uncertainties, as one may estimate it due to the fluctuations of values between experiments and the quality of the global fit, it is clear that the uncertainty obtained from the standard $\Delta\chi^2$=1 condition, shown in tab.3 is unrealistically small. In fact, the range of variation of α_s obtained

	$\alpha_{s_{min}}$	$\Delta\chi^2 = 1$	$\Delta\chi^2 = 100$	# pt
TOT (all exp)	0.120	$\pm$0.0004	$\pm$0.004	3382
NMC-pd	0.125	$\pm$0.002	$\pm$0.019	153
NMC	0.129	$\pm$0.002	$\pm$0.023	245
SLAC	0.125	$\pm$0.003	$\pm$0.026	93
BCDMS	0.118	$\pm$0.001	$\pm$0.008	581
ZEUS	0.120	$\pm$0.001	$\pm$0.012	507
H1	0.120	$\pm$0.001	$\pm$0.009	632
CHORUS	0.122	$\pm$0.001	$\pm$0.009	942
FLH108	0.127	$\pm$0.010	$\pm$0.104	8
NTVDMN	0.118	$\pm$0.003	$\pm$0.027	84
XF3GZ	0.117	$\pm$0.009	$\pm$0.091	8
ZEUS-H2	0.115	$\pm$0.002	$\pm$0.018	127

Table 3: Values of α_s and its 68% CL uncertainty obtained from the parabolic fit displayed in fig.18. The range of α_s obtained from $\Delta\chi^2 = 100$ is also shown. The last column shows the number of data points for each experiment.

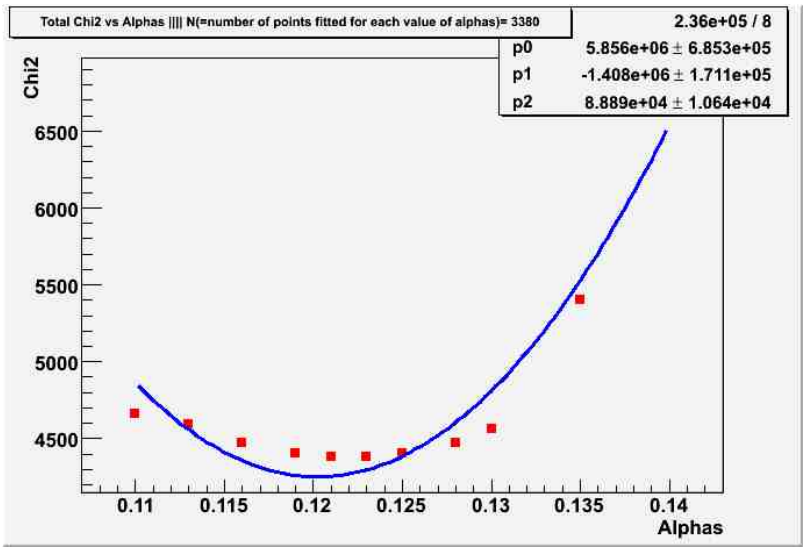

Figure 6: Parabolic fit to the global χ^2 values in the case of 500 MonteCarlo replicas.

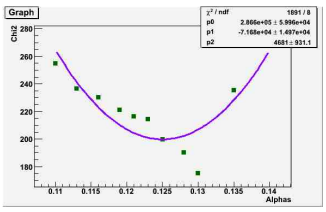

Figure 7: NMCpd $\alpha_{s_{min}} = 0.125$

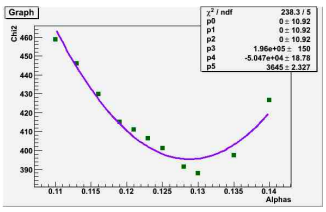

Figure 8: NMC $\alpha_{s_{min}} = 0.129$

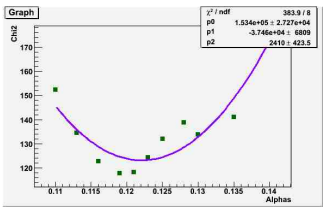

Figure 9: SLAC $\alpha_{s_{min}} = 0.122$

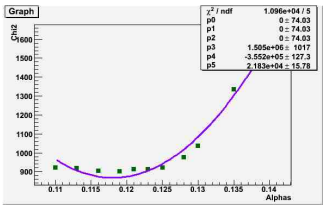

Figure 10: BDCMS $\alpha_{s_{min}} = 0.118$

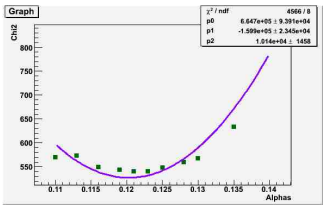

Figure 11: ZEUS $\alpha_{s_{min}} = 0.120$

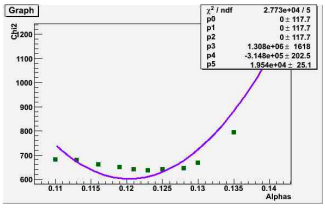

Figure 12: H1 $\alpha_{s_{min}} = 0.120$

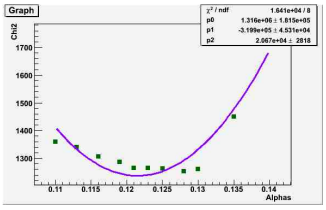

Figure 13: CHORUS $\alpha_{s_{min}} = 0.122$

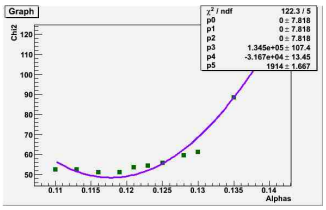

Figure 14: NTVDMN $\alpha_{s_{min}} = 0.118$

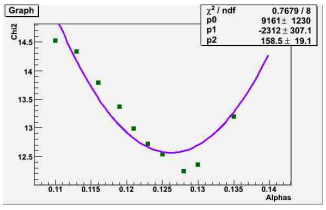

Figure 15: FLH108 $\alpha_{s_{min}} = 0.126$

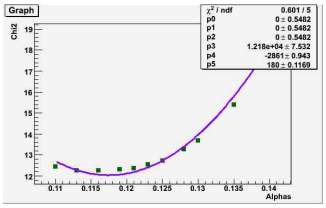

Figure 16: XF3GZ $\alpha_{s_{min}} = 0.117$

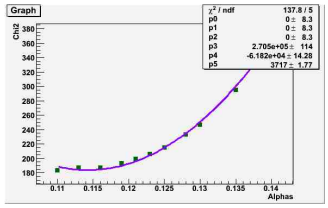

Figure 17: ZEUSH2 $\alpha_{s_{min}} = 0.115$

Figure 18: Parabolic fit based on the χ^2 for each experiment from tab.2.

allowing $\Delta\chi^2$=100 (also shown in tab.3) seems a more realistic estimate of the uncertainty. We may obtain a more reliable determination of α_s by using the available points to construct an ensemble of determinations of α_s. The we can determine *best-fit* α_s and its uncertainty by performing statistics on this ensemble, thereby controlling fluctuations as follows:

1. we have determined all the possible subsets of three elements, picking them up from the original ensemble containing the eleven chosen α_s values (0.110, 0.113, etc...) and their corresponding global fit χ^2 ;

2. for each one of these subsets (165 in all, as they correspond to the combination of 11 objects taken 3 at a time), we have made a parabolic fit;

3. for each parabolic fit we have determined the minimum and the half-width at a distance equal to 1 ($\Delta\chi^2$=1 rule) from the minimum;

4. we have calculated the averages of these three quantities, which, from now on, will be denoted as:
   $\langle\alpha_{s_{500}}\rangle$= average of the 165 values of α_s;
   $\langle\Delta\chi^2 = 1_{500}\rangle$ = average of the 165 half-widthes obtained from $\Delta\chi^2$=1 rule;
   we have also determined the standard deviation of the 165 $\Delta\chi^2$=1 values obtained; this quantity will be denoted by the symbol $\sigma_{\Delta\chi^2=1_{500}}$.

The results are listed below:

$\langle\alpha_{s_{500}}\rangle$	0.1197
$\langle\Delta\chi^2 = 1_{500}\rangle$	0.0016
$\sigma_{\Delta\chi^2=1_{500}}$	0.0013

This procedure is conceptually very close to the MonteCarlo technique, where the place of replicas has been taken by subsets: we have eleven original data points, providing for α_s a single unstable measure 0,120 $\pm$ 0.0016; we thus consider all possible three points subsets, each one with its α_s best-value; since each one of these values can be regarded as an independent "measure" for α_s, their average will be the best estimation we can obtain. Therefore results in table 3.2.2 can be interpreted as follows:

- $\langle\alpha_{s_{500}}\rangle$ is our *best-fit value of* α_s;
- $\langle\Delta\chi^2 = 1_{500}\rangle$ is our best estimate for the 68% CL;
- $\sigma_{\Delta\chi^2=1_{500}}$ is the uncertainty on α_s due to statistical fluctuations; it then represents the uncertainty given by the procedural limitations.

This interpretation is confirmed by the results, displayed below, obtained by performing this procedure with a sensibly smaller number of replicas, namely 100 replicas: As a matter of fact, by switching from 100 to 500 repli-

$\langle \alpha_{s_{100}} \rangle$	0.1110
$\langle \Delta\chi^2 = 1_{100} \rangle$	0.0018
$\sigma_{\Delta\chi^2=1_{100}}$	0.0016

cas, $\langle \alpha_{s_{100}} \rangle$ shifts towards the conventionally accepted value $\alpha_s(M_z^2)$=0.119 and at the same time, the uncertainty $\sigma_{\Delta\chi^2=1_{100}}$, to which we attributed the meaning of error intrinsic to the procedure, slightly decreases, thus confirming this interpretation.

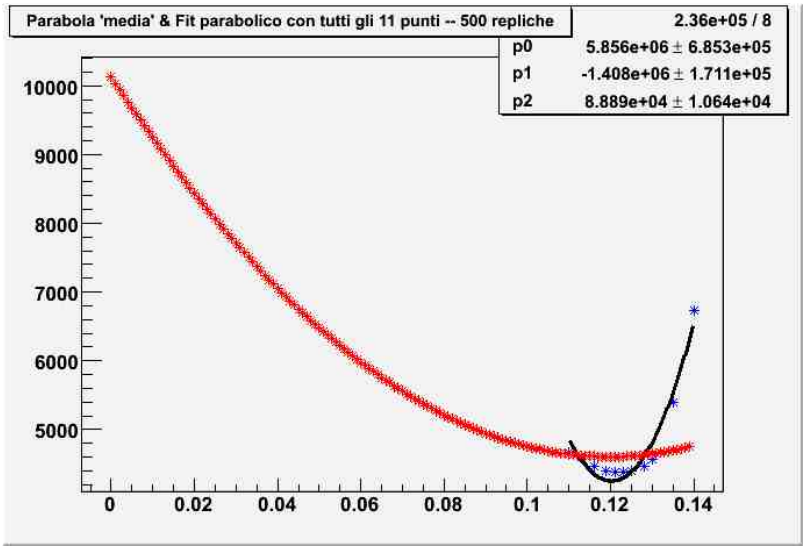

Figure 19: In black the parabola obtained by simply fitting the eleven data points and in red the 'average' parabola, drawn by using the average values ($\langle \alpha_{s_{500}} \rangle$ as point of minimum and $\langle \Delta\chi^2 = 1_{500} \rangle$ as half-width at a distance 1 from the minimum).

From fig.19 we can directly see the great difference between the experimental uncertainties ($\Delta\chi^2 = 1$)=0.0004 and $\sigma_{\Delta\chi^2=1,100}$=0.0016, here represented by the widths of the parabolas, determined respectively with the first and the second procedure described above. This provides further evidence that the second procedure is appreciably better than the first one, since it provides both an acceptable experimental uncertainty for α_s and a procedural error, which we could not access with the first procedure. Fig.20 instead, shows that the distribution of the 165 $\Delta\chi^2$=1, i.e. of the errors of 165 'virtually independent' measures of αs, is approximately gaussian. Therefore we have the guarantee that we can properly consider $\langle \Delta\chi^2 = 1_{500} \rangle$, i.e. the

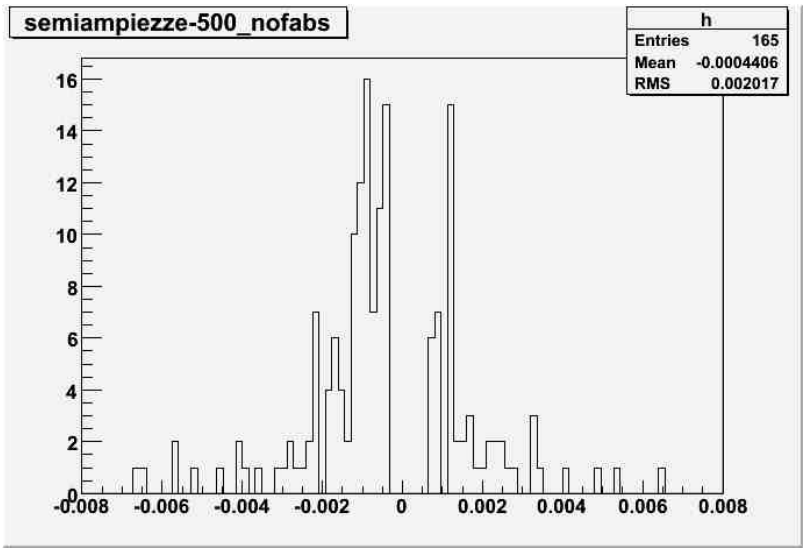

Figure 20: Histogram illustrating the distribution of the 165 $\Delta\chi^2$=1 values around their mean 0.0016

FWHM of this gaussian, as the uncertainty connected to this ensemble of measures.

Conclusion

We have presented a determination of the strong coupling α_s performed by using the NNPDF methodology, starting from almost the totality of DIS data available up to now. The determination has required some steps, which have finally led, from a global parton analysis, to the result $\alpha_s(M_z^2) = 0.1197 \pm 0.0016^{stat} \pm 0.0013^{syst}$. On top of that, the parton analyses based on data from single DIS experiments have shown that the coupling can be determined separately from each one of them. The value of the coupling is very close to the current global average; its uncertainties are of two different kinds:
- 0.0016, denoted by *statistical error*, represents experimental uncertainties, i.e. the fact that each experiment does not measure the exact value of the considered physical quantity, but a different value on the basis of the probability distribution of errors. In this sense this *statistical error* is connected to the statistical fluctuations which dominate experiments;
- 0.0013, denoted by *systematic error*, represents the uncertainties due to the procedure used to determine α_s. In particular this uncertainty is due to the procedural limitation determined by the choice of the number of MonteCarlo replicas used in the NNPDF parton fits. Therefore the result of this analysis can't be considered definitive. If we broaden the amount of

experimental data and we increase the number of MonteCarlo replicas both the statistical and the systematical error will get smaller.

References

[1] B. Pohv, K. Rith, C. Scholz, F. Zetsche, *Particles and Nuclei. An Introduction to the Physical Concepts*, Springer (1995).

[2] G. D. Coughlan, J. E. Dood, *The Ideas of Particle Physics*, Cambridge University Press (1991).

[3] C. Amsler *et al.*, 2008 Review of Particle Physics, Chapter 14: 'The Quark Model', Physics Letter **B667**, 1 (2008).

[4] C. Amsler *et al.*, 2008 Review of Particle Physics. Chapter 9: 'Quantum Chromodynamics and its coupling, Physics Letter **B667**, 1 (2008).

[5] http://sophia.ecm.ub.es/nnpdf .

[6] NNPDF, *A determination of parton distributions with faithful uncertainty estimation*, arXiv:0808.1231v4[hep-ph].

[7] NNPDF, L. Del Debbio *et al.*, *Neural Network determination of parton distributions:the non singlet case*, arXiv:0701127v1[hep-ph].

[8] A. D. Martin, W. J. Stirling, R. S. Thorne, G. Watt, *Uncertainties on α_s in global PDF analyses*, arXiv:0905.3531v1[hep-ph].

Acknowledgements

First, I would like to thank Professor Stefano Forte for having explained me with infinite patience the basis concepts of QCD, which represented a totally new world to me, and for having taken the burden of teaching to the undersigned how to write a scientific text with great dedication and precision. This work would have never become a real scientific thesis without his help. Then I would like to thank Doctor Juan Rojo for having followed me in the concrete realization of this analysis wih great passion and for the constant help he gave me when I encountered problems which seemed unsolvable to me.
Of course I want to thank my parents for their support at home and for having patiently listened to my complaints when something went wrong. Finally I must thank all my friends for their carefree cheerfulness, which has always been the best medicine when bad moments occurred.